Experiments in Fluids 31 (2001) 567–578 © Springer-Verlag 2001

Measurement of flows around modern commercial ship models

W. J. Kim, S. H. Van, D. H. Kim

Abstract To document the details of flow characteristics around modern commercial ships, global force, wave pattern, and local mean velocity components were measured in the towing tank. Three modern commercial hull models of a container ship (KRISO container ship = KCS) and of two very large crude-oil carriers (VLCCs) with the same forebody and slightly different afterbody (KVLCC and KVLCC2) having bow and stern bulbs were selected for the test. Uncertainty analysis was performed for the measured data using the procedure recommended by the ITTC. Obtained experimental data will provide a good opportunity to explore integrated flow phenomena around practical hull forms of today. Those can be also used as the validation data for the computational fluid dynamics (CFD) code of both inviscid and viscous flow calculations.

1 Introduction

As most cargo worldwide today is transported via ship, it is very important to design the ship hull forms such that they operate economically. To propel a ship, its engine has to provide enough power to overcome the hydrodynamic drag due to viscosity and wave generation. It is necessary to understand the complicated flow characteristics to design the hull forms with lower drag and higher propulsive efficiency. For better understanding of the flow around a modern commercial ship, it is of primary importance to produce reliable experiment data of practical hull forms. The experiment data describing the local flow details are also invaluable in the field of computational fluid dynamics (CFD) for the validation of the developed physical and numerical modeling.

There have been some experimental data for the flows around ship models. The International Towing Tank Conference (hereafter, ITTC) summarized available benchmark database for CFD validation for resistance and propulsion of a ship (ITTC 1999; see also Longo and Stern 1996; Stern et al. 1998). For the cargo-container ship, Series 60 (Fry and Kim 1985; Toda et al. 1990, 1992; Longo et al. 1993; Suzuki et al. 1997) and Hamburg Test Case (Bertram et al. 1994; Gietz and Kux 1995) are given. DTMB model 5415 is recommended for a combatant model (Fry and Kim 1985; Ratcliffe 1998; Olivieri and Penna 1999; Longo and Stern 1999). For the full-form tanker, HSVA/Dyne tanker models (Knaack 1992; Denker et al. 1992; Dyne 1995) and Ryuko-Maru (Ogiwara 1994; Suzuki et al. 1998) are given. Previously, two workshops (Larsson et al. 1991; Kodama 1994) were arranged for the computational analysis of flow around a ship, and HSVA/Dyne tanker models and a Series 60 model were chosen for the test cases. However, those data are often partial and not enough to understand the complicated flow phenomena. The hull forms used in those experiments are old-fashioned and quite different from the modern hull forms of ships today.

The aim of the present study is to provide a set of experimental data for the modern commercial hull forms with bulbous bow and stern bulb. The experimental data presented in this paper encompass resistance and propulsive efficiency, wave elevation along the hull surface, wave pattern along longitudinal and transverse cuts, and mean velocity components in boundary layer and wake. Measurements were performed in the towing tank of Korea Research Institute of Ships and Ocean Engineering (hereafter, KRISO).

It is desirable to select the actual hull forms built by a shipyard and subjected to sea-trial; however, they can hardly be disclosed. Instead, the hull forms for the container ship and the VLCC (very large crude-oil carrier) were designed by KRISO. In the case of the container ship, it was designed to carry 3,600 containers, while the VLCC was supposed to transport 300,000 tons of crude oil. For the VLCC, two hull forms with the same forebody and slightly different afterbody were designed to identify the stern flow change due to hull form variation. For briefness, the 3600TEU container ship was named KCS and the two 300 KVLCCs were named KVLCC and KVLCC2, respectively. Their main particulars and hull geometries are very close to those of the commercial ships today. For KCS with moderate speed and low block coefficient, wave generation on free surface was of the primary interest, since the big bulbous bow was supposed to suppress bow wave generation and the flat stern overhang and the transom stern produced very complicated stern waves. On the other hand, for KVLCC and KVLCC2 with low speed and large

Received: 26 September 2000/Accepted: 22 May 2001

W. J. Kim (✉), S. H. Van, D. H. Kim
Korea Research Institute of Ships and Ocean Engineering
KORDI, Jang-Dong 171, Taejon, 305–343, Korea
e-mail: wjkim@kriso.re.kr

The present work was based on the project "Improvement of Resistance Performance of Commercial Ships," supported by the Ministry of Trade and Industry of Korea. The authors thank the technicians of the KRISO towing tank for their valuable contribution in manufacturing models and helping in experiments. The hull information and experiment data discussed in this paper are available at http://hyperteam.krio.re.kr.

block coefficient, viscous boundary layer flow in the stern region was focused upon, since strong bilge vortices were entering into the propeller plane.

Recently the Gothenburg 2000 Workshop on CFD in ship hydrodynamics chose three test ships (Larsson et al. 2000), one was the DTMB model 5415 combatant model mentioned earlier and the others were the KCS and KVLCC2 of the present paper. International collaborative works were performed to provide the well-prepared data set to the ship hydrodynamics community for the CFD validation. The Ship Research Institute of Japan measured stern flow field and surface pressure distribution with and without propeller rotating behind the KCS model (Fujisawa et al. 2000; Tsukada et al. 2000). For the KVLCC2 model, wind tunnel experiments were carried out for turbulence quantities (Lee et al. 1998; Van et al. 1999). In the present paper, the experimental procedures and the measured data for KCS, KVLCC, and KVLCC2 procured in the KRISO towing tank are described. The hull forms and measured data presented in this paper are publicly available in the Internet (http://hyperteam.kriso.re.kr or http://www.iihr.uiowa.edu/gothenburg2000/).

In the following, the hull forms and experimental apparatus used to document global force, wave pattern, and local velocity field are given along with the uncertainty analysis results based on the procedure recommended by ITTC (ITTC 1999; Coleman and Steele 1999). Measured resistances, wave profiles along the hull surfaces, wave patterns obtained from transverse, and longitudinal cut methods are discussed, followed by the mean velocity fields around the stern region. For the VLCC models with stern frame line modification, the propeller plane wakes are also analyzed with the viewpoint of propulsive efficiency as well as resistance, since the effect of stern hull form variation on the speed of a ship should be considered as an outcome of both resistance and propulsion characteristics. As proven in the Gothenburg 2000 Workshop, authors expect the present data to be useful for the understanding of the flows around modern commercial hull forms and also for the validation of CFD tools in ship hydrodynamics.

2 Experimental apparatus

2.1 Model ships

In the present experiment, three test hull forms were selected, i.e., a 3600-TEU container ship and two 300 KVLCCs, recently designed by KRISO. The test ships are of very similar shapes to commercial ships today. Tables 1, 2 and 3 provide the principal particulars of the test ships, whose body plans and side profiles are also given in Figs. 1 and 2.

Initially, three hull forms were designed and resistance/self-propulsion tests were performed for the container ship (Kang et al. 1998). Of the three container hull forms, F1 + A2 (i.e., the first forebody and the second afterbody) was selected for local flow measurement and named KCS, meaning KRISO container ship. For the VLCC, two hull forms with the same forebody (F1) and slightly different afterbody geometries (A1 and A2) with the same side profile were designed and used for the global-force and local-flow measurement.

Table 1. Principal particulars of KCS

Designation	Prototype	TT model
Scale ratio	1.0	1/31.6
Speed (m/s)	12.3467	2.1964
Froude number (*Fn*)	0.26	0.26
Reynolds number (*Re*)	2.4×10^9	1.4×10^7
Length (m)	230.0	7.2786
Breadth (m)	32.2	1.0190
Depth (m)	19.0	0.6013
Draft (m)	10.8	0.3418
Wetted surface area (m^2)	9,498.0	9.5121
Displacement (m^3)	52,030.0	1.6490
Block coefficient (C_B)	0.6505	0.6505

Table 2. Principal particulars of KVLCC

Designation	Prototype	TT model
Scale ratio	1.0	1/58.0
Speed (m/s)	7.9739	1.047
Froude number (*Fn*)	0.142	0.142
Reynolds number (*Re*)	2.1×10^9	4.6×10^6
Length (m)	320.0	5.5172
Breadth (m)	58.0	1.0
Depth (m)	30.0	0.5172
Draft (m)	20.8	0.3586
Wetted surface area (m^2)	27,320.0	8.1213
Displacement (m^3)	312,737	1.6029
Block coefficient (C_B)	0.8101	0.8101

Table 3. Principal particulars of KVLCC2

Designation	Prototype	TT model
Scale ratio	1.0	1/58.0
Speed (m/s)	7.9739	1.047
Froude number (*Fn*)	0.142	0.142
Reynolds number (*Re*)	2.1×10^9	4.6×10^6
Length (m)	320.0	5.5172
Breadth (m)	58.0	1.0
Depth (m)	30.0	0.5172
Draft (m)	20.8	0.3586
Wetted surface area (m^2)	27,194.0	8.0838
Displacement (m^3)	312,621	1.6023
Block coefficient (C_B)	0.8098	0.8098

The two VLCC hull forms, i.e., F1 + A1 and F1 + A2, were named KVLCC and KVLCC2, respectively. The first VLCC stern hull form (A1) has barge-type stern frame lines with a fine stern bulb, while the second stern hull form (A2) has more U-shaped stern frame lines than the former. Recently, CFD tools are being used in the initial design stage in order to evaluate the resistance performance and wake distribution of hull forms in shipyards. It is often asked if the computational tools can tell the flow difference from the frame line changes the designer actually applies during the hull form optimization. To fulfill the aforementioned request, the experimental data for CFD validation should be for comparative purposes like the flow measurements around two slightly different hull

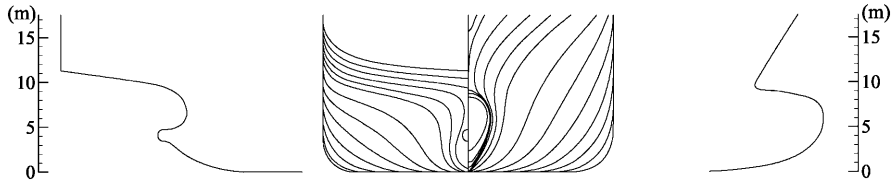

Fig. 1. Body plan and side profile of KCS

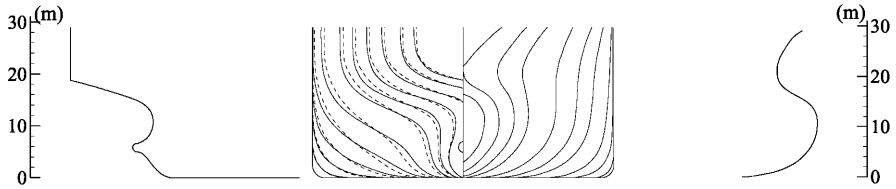

Fig. 2. Body plans and side profiles of KVLCC and KVLCC2 (*Soild lines*: KVLCC, *Dotted lines*: KVLCC2)

forms. The hull form changes of VLCC sterns (A1 and A2) correspond to those shipyards usually apply, which ensures the usefulness of the present data in the evaluation of CFD tools for wake prediction.

For the towing tank test, a model of the KCS was made of wood with a scale ratio of 1/31.6, while the two models of KVLCC and KVLCC2 were quite small with a scale ratio of 1/58 in order to keep the width of the models accommodated in the measurement frame. Studs with trapezoidal heads as turbulence stimulators were nailed at St. 19 and at the middle of the bow bulb at 10-mm girthwise intervals, so as to make sure that the flow became fully turbulent. In shipbuilding engineering, St. 0 and St. 20 mean the after perpendicular (A.P.) at the stern and the forward perpendicular (F.P.) at the bow of a ship, respectively. Stations and waterlines were marked densely to locate the probes in the proper positions and to make it easy to read wave profiles along the hull surface. The model ship was fixed at the towing carriage by using two clamping devices located around St. 6 and St. 14. All the local flow measurements in the towing tank were carried out in the fixed condition, where neither trim nor sinkage was allowed, in order to prevent the ship model from breaking the probes. Besides, the computational condition is easier in the fixed condition, since the posture of ship does not change during the run.

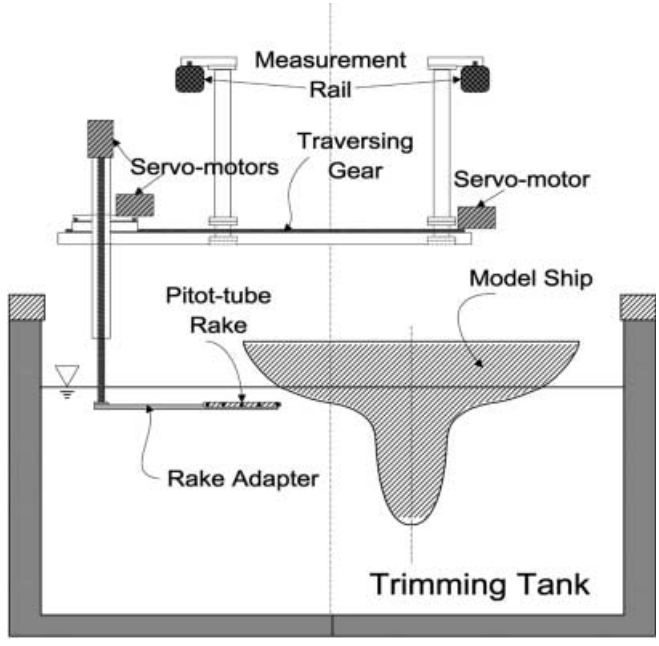

Fig. 3. Schematics of towing tank measurement frame

2.2
Towing tank

The measurement of global force, wave pattern, and mean velocity components were carried out in the towing tank of KRISO. The size of the towing tank is 200 m × 16 m × 7 m (length × width × depth) and the towing carriage can run up to 6 m/s. Blockage coefficients, defined as the ratio of the sectional area of the model and the towing tank, were less than 0.35% for all test models, allowing the blockage effect to be ignored.

To keep the side of model ship spacious, the ship model was moved into the starboard direction by 25 ~ 30 cm from the center of the measurement frame, so that the probe-holding device connected to the traversing mechanism could be accommodated, as shown in Fig. 3. The traversing mechanism driven by three servomotors with a precision of 0.02 mm for each direction was installed at the measurement rail to position the probes accurately and efficiently.

3
Measurement and uncertainty analysis

In the towing tank test, a model ship was towed at the speed of Froude's similarity law such that the speed ratio of the model and the prototype is the square root of the scale ratio. Since the design speed (V_S) of the KCS was 12.247 m/s (i.e., 24.0 knots), the model ship was towed at the speed (V_M) of 2.196 m/s. The resulting Froude number ($Fn = V_S/\sqrt{(gL_{pp})_S} = V_M/\sqrt{(gL_{pp})_M}$) was 0.26. The corresponding Reynolds number ($Re = V_M\,(L_{pp})_M/v$) of the KCS model was 1.4×10^7. Here, $(L_{PP})_S$ and $(L_{PP})_M$ are the length between perpendiculars of the prototype and the model ship, respectively. g is the gravitational acceleration and v is the kinematic viscosity. For KVLCC and KVLCC2, the Froude number was 0.142 and the speeds of the prototype and the model were 7.974 m/s (i.e., 15.5

knots) and 1.047 m/s, respectively. The Reynolds number of both KVLCC and KVLCC2 models was 4.6×10^6.

3.1
Global-force measurement

The total resistance (drag) coefficients were measured using the resistance dynamometer (R25, Kempf and Remmers, Hamburg, Germany). When a ship is running, its posture is changed. The trim and sinkage are usually allowed in the towing tank resistance test to match the real situation (i.e., free condition). However, in the present study, trim and sinkage were not allowed in the local flow measurement (i.e., fixed condition). It is not easy to measure drag in the fixed condition since the fixing device can easily disturb the axial force balance. Thus, in the resistance measurement, negative trim and sinkage was initially given to make the fixed running condition. Initially, the weight distribution for the model ship was adjusted to have the negative amount of trim and sinkage of the free condition to obtain the resistance in zero trim and sinkage. After several iterations, the resistance coefficient could be procured in zero trim and sinkage condition.

The measured total resistance coefficients were divided into frictional resistance coefficients, based on the 1957 ITTC formula (SNAME 1967), and residuary resistance coefficients representing the sum of wave-making drag and form drag. The measured residuary resistance coefficient of KCS at design speed was 0.725×10^{-3}, while those of KVLCC and KVLCC2 were 0.638×10^{-3} and 0.660×10^{-3}, respectively. The frictional resistance coefficient of KCS from the 1957 ITTC formula was 2.832×10^{-3}, while those of KVLCC and KVLCC2 were both 3.450×10^{-3}.

The self-propulsion test with rotating propeller was also carried out for KVLCC and KVLCC2 to compare the propulsive efficiency of the two hull forms. The stern hull form change usually modifies the wake distribution at the propeller plane. Thus, the propeller inflow condition becomes different. A model propeller formerly used for the similar VLCC was chosen for the assessment of the final propulsive power of the two VLCCs. To achieve the self-propelled condition in the towing tank, the towing rod provided the difference of frictional resistance coefficients between the prototype and the model ship, while the remaining drag was overcome by the thrust from the propeller. The thrust and torque dynamometer (NR330, Kempf and Remmers) was utilized. The measured propulsive efficiency and the resulting power for the prototype will be discussed in Sect. 4.2.2 with the local flow measurement results.

3.2
Wave pattern measurements

The servo-needle-type wave height gauges (SHT3–30, West Japan Fluids Engineering Laboratory Co., Nagasaki, Japan) were used to document the full spectrum of generated waves. First of all, the longitudinal cut method was utilized to measure the generated waves along $36 \sim 39$ lateral positions. Three gauges were tied up in one unit, so that three lines of wave height data could be obtained in a single run. The wave height gauge holder, driven by an electric motor, could slide along a truss attached at the sidewall of towing tank. An optical switch at 3 m ahead of F.P. provided the triggering signal to identify the relative location between the model ship and the wave height gauges. Data were obtained at the rate of $50 \sim 100$ Hz using a portable analog-digital converter (DaqBook, IO-Tech, Cleveland, Ohio) for 50 s. The duration of sampling was long enough to include the reflected waves from the sidewall of the towing tank. The servo-needle-type wave height gauges attached to the cantilever truss for the wave measurement along longitudinal cuts are shown in Fig. 4.

Next, waves around the bow and stern region were measured by the transverse-cut method using the gauges attached to the traversing mechanism moving with the towing carriage. In the case of the KCS having a large angle of bow flare, a gauge was inclined by 19° to access close to the hull surface. To measure bow and stern waves, two or three wave gauges were attached to the traversing mechanism and moved after gathering 100 samples in 5 s at each position. It was found that the measured wave height behind the stern was hardly stable, especially for the KCS. The data given here for the bow and stern region other than the longitudinal cuts are simply averaged at each position.

On the other hand, to measure the wave elevation along the hull surface, a telescope, a digital video recorder, and a still camera were used. It was very difficult to read the wave elevation near the stern area, since waves along the flat overhang near the design waterline were not clearly seen. To reduce human error, three persons used three different means to read the elevation and the average value was taken as the wave elevation along the hull surface.

3.3
Local mean velocity measurements

For the measurement of the three-dimensional mean velocity field around stern region, a 5-hole Pitot-tube rake was utilized. The rake included five 5-hole Pitot tubes with 4 cm intervals to speed up the measurement as shown in Fig. 5. An adapter was designed to connect the rake to the three-dimensional traversing mechanism installed at the

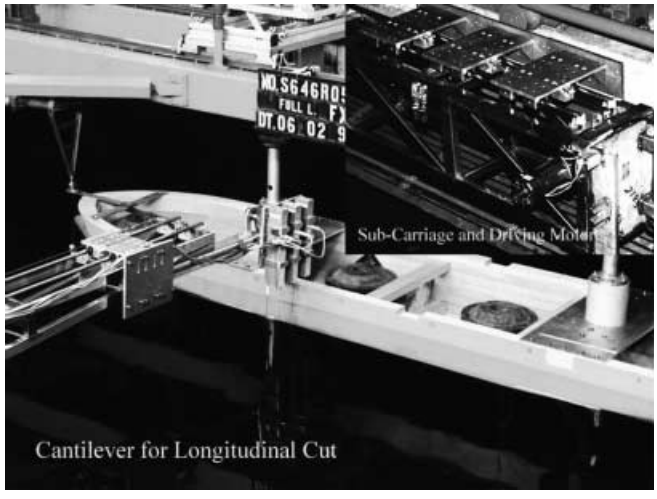

Fig. 4. Photograph of wave measurement along longitudinal cuts

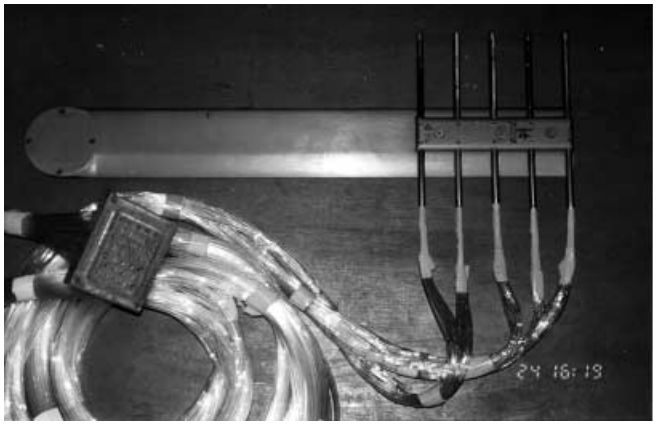

Fig. 5. Pitot-tube rake used to measure the velocities in the towing tank

towing carriage. Before and after the local flow measurement, the nulling procedure without the model ship was completed to confirm and adjust the Pitot-tube rake setting. The 5-hole Pitot tube had a semi-spherical tip and the outer diameter of the tube was 8 mm. Before the measurement, the Pitot tubes were calibrated in the range of ±40° for both pitch and yaw angles simultaneously. The calibration device provided first the pitch (vertical) angle and then the yaw (horizontal) angle, which resulted in pitch-yaw chart calibration (Kim et al. 1997). A total of 121 angle variations, i.e., 11 angles both for pitch and yaw, provided three correlation coefficients for velocity magnitude, pitch, and yaw angle, respectively.

Each tube was connected directly to a Validyne pressure transducer (DP-15) and carrier demodulator (CD-10). An analog–digital signal converter (NEFF) on the towing carriage provided pressure data to compute three-dimensional velocity components. A pressure signal from each hole of the tube was obtained for 8 s at a rate of 50 Hz and then averaged. Calculated correlation coefficients were used to determine the magnitude and angle of the local flow, utilizing the already obtained calibration chart. Bicubic spline interpolation was used to find the correlation coefficients of the corresponding calibration angles.

It was possible to obtain data at $3 \sim 6$ positions during one carriage run, depending on the model ship speed. However, local flow angles were sometimes outside of the calibration ranges of ±40° of pitch and yaw angles, especially below the stern cap and behind the transom. If the local flow angle was outside of the calibration range, the measured data was discarded and velocity components could not be determined at those positions. This happened when the axial velocity component was relatively small but the transverse flow angle was large. Measurements were carried out at five planes (St. 2, 1, 0.35, −0.5767, −2) for the KCS and at six planes (St. 3, 2, 1, 0.35, −0.4525, −2) for both KVLCC and KVLCC2.

3.4
Experimental uncertainties

Uncertainty analysis was performed for the measured data following the procedure recommended by ITTC (1999). For the resistance test, uncertainty analysis had already been performed (Van and Park 1993) and was not repeated in the present study. The uncertainty interval with 95% confidence level of resistance measurement was about 1.0% of the total resistance, including both bias and precision errors.

In the case of wave height measurement, two different methods were used. When obtaining the hull surface profile, the major source of error stems from the human eye, because wave heights were read from the photo, video, or by telescope during running. The bias error for the wave elevation along the hull surface was within 1.0 mm, except for F.P., where the wave itself tended to move up and down by a few millimeters during the test. For the wave measurement along the longitudinal cuts, the oncoming waves (time-varying quantity) were measured. Thus, the precision error was not taken into account. The bias error came from the nonlinearity and resolution of servo-needle-type gauge and amplifier. The location of wave probes (initial setting and movement), and the phase due to the triggering signal were also taken into consideration. The resulting bias error was within 0.5 mm for the wave height along longitudinal cuts.

For local mean velocity measurement, both bias and precision errors were considered. As sources of bias error, the resolution and nonlinearity of pressure transducers, demodulators, A/D converters, the location of the probes, the carriage speed, and the water temperature and density were considered. The bias error was found to be less than 0.1% of the model speed. The precision error was estimated from the measured data series for each probe location. The time history of the measured data showed that the pressure value near the hull surface and behind the hull body was quite unstable, however, it became very stable in the outside region. The precision error was much larger than the bias error. The resulting error with 95% confidence interval was ±0.8% of the model speed in the near-wall region and ±0.3% in the outside region. However, it became ±1.2% at a very few points just behind the stern bulb and transom.

4
Results

In the following, the measured wave patterns and local mean velocity components are given. The Cartesian coordinates (X,Y,Z) are used for displaying the data, where X denotes the downstream direction, Y starboard, and Z the upward direction. The origin of the coordinates is located at midship and on a calm free surface. All the coordinates are nondimensionalized by the length between perpendiculars ($(L_{pp})_M$) of the model ships. U, V, and W denote the mean velocity components in the X, Y, and Z directions, non-dimensionalized by the towing carriage speed (V_M).

4.1
Wave patterns

When a ship advances in calm water, it generates waves on the disturbed air–water interface (free surface). The ship has to supply energy continuously to the generated wave pattern following the ship. Thus, the ship should overcome the drag induced by the wave generation on the free sur-

face. The so-called wave resistance (drag) related to this phenomenon is important in ship design.

Modern commercial ships have a bulbous bow to reduce wave generation around the bow region. The waves generated by the bow bulb under the free surface interact with the waves generated near the design waterline. It is believed that wave resistance can be reduced if the bow bulb is properly located. The generated waves can be divided into transverse and divergent wave components depending on the wave-propagating direction. The transverse wave components have the crest line normal to the X-direction with the phase velocity similar to the ship speed, while the divergent wave components are located at the edge of the so-called Kelvin triangle with the shorter wavelength and slower phase velocity (SNAME 1967). However, in reality, it is not easy to clearly identify the two components of the waves generated, since the waves are seen in superposed form.

There are some efforts to figure out the generated wave patterns around a hull form by using CFD techniques. The wave measurements for the KCS and the VLCCs provide severe test cases for wave resistance prediction, since they contain various aspects of the free-surface phenomena around modern commercial ships. Viscous or inviscid flow solvers with the capability of handling the nonlinear free-surface condition can be validated against the present data to prove the accurate prediction of free-surface flow around an actual hull form.

4.1.1
The KCS case

Before the global wave pattern is explored, the wave profile along the hull surface of the KCS is given in Fig. 6. The Froude number of the experiment was 0.26, thus the corresponding length of transverse wave propagating with the ship speed is $2\pi Fn^2$, i.e., 0.425 for this case. About two principal wavelengths are expected along the hull surface. The crests are located at $X = -0.475$ and 0.05, while the troughs are seen at $X = -0.15$ and 0.25. The first crest is over 1% of the ship length, while the first trough is −0.5%. It is observed that a small wave from the forebody shoulder exists at $X = -0.4$ just after the first crest. The wave elevation near the stern is much flatter than in the bow region. The thick boundary layer existing around the stern region suppresses the pressure recovery and restrains the wave rising. Moreover, modern container ships like the KCS usually have the flat overhang pushing down the water surface in the stern region.

The global view of the wave pattern of the KCS is shown in Fig. 7. It should be noted that only the port side was measured and reflected on the starboard side for plotting. It is observed that a wave exists inside a certain angle known as the Kelvin angle from linear potential wave theory. The bow wave having the maximum height on the hull surface gradually disappears, followed by a trough and crest lines of divergent wave components with decreasing amplitude along the edge of the wave region. Transverse wave components are seen inside the divergent wave patterns.

An interesting phenomenon in this wave pattern around the KCS occurred behind the transom stern. When the ship was at rest, the transom stern was above the calm water surface, since the design waterline was located below the transom. However, as the ship advanced and reached steady state at the design speed, the generated wave rose over the transom stern. If the speed of the ship is high, the wave surface would be parallel to the hull surface under the transom stern. Thus, the transom stern could appear out of water region, resulting in the so-called "dry transom". When the speed of the ship is very low, wave generation could be ignored. However, if the ship advances at

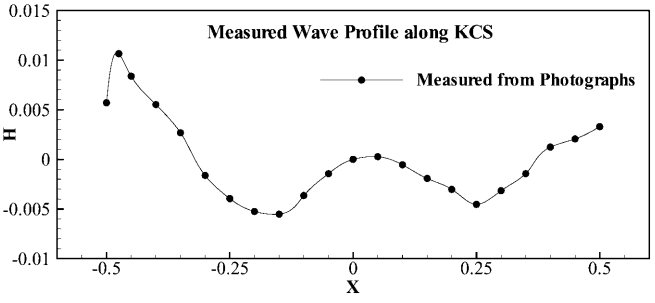

Fig. 6. Measured wave elevation along KCS ($Fn = 0.26$)

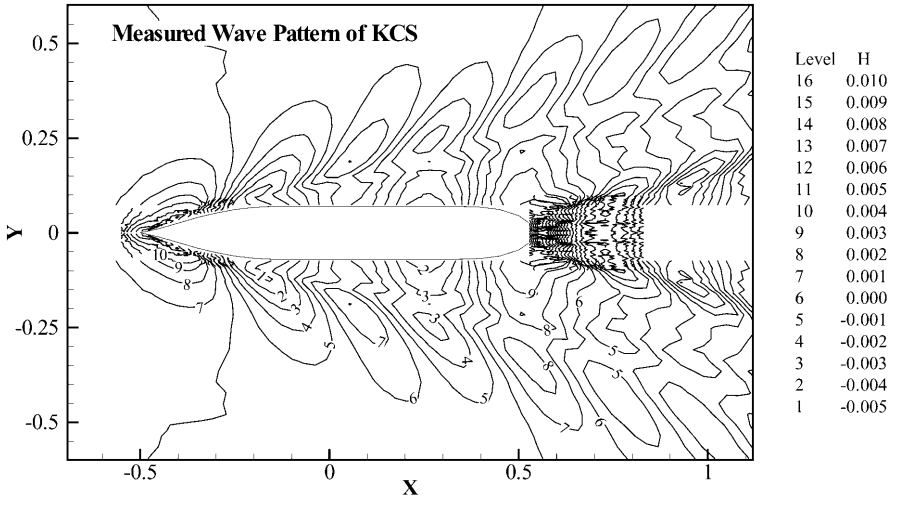

Level	H
16	0.010
15	0.009
14	0.008
13	0.007
12	0.006
11	0.005
10	0.004
9	0.003
8	0.002
7	0.001
6	0.000
5	-0.001
4	-0.002
3	-0.003
2	-0.004
1	-0.005

Fig. 7. Measured wave pattern around KCS ($Fn = 0.26$)

the moderate speed as in the present KCS case, waves rising over the transom stern and flow reversal behind the transom make an unsteady and complicated wave pattern, as shown in Fig. 7. It is observed that the wave surface looks like unsteady bubbling up behind the transom. In Fig. 7 the hull line is the intersection of the real free surface, where the effect of the transom stern is clearly identified. It will be quite difficult to apply numerical modeling to the unstable wave pattern behind the transom as described above. However, the apparent wave pattern generated by the real container ships today is very similar to the present results.

4.1.2
The KVLCC and KVLCC2 cases

Most VLCC hull forms have a large block coefficient over 0.8 with a full bow shape and long parallel middle body. The wave pattern generated by VLCC hull forms with a low Froude number can be characterized by a big bow wave followed by much smaller waves. Wave elevations along the hull surfaces of KVLCC and KVLCC2 are compared in Fig. 8. The discrepancy in the forebody should be considered as a measurement uncertainty since the forebodies of the two VLCC hull forms are the same. There is a small difference around $X = 0.3$ due to the slight difference in waterline angle of the two ship models. Wave patterns are compared in Fig. 9. It should be noted that the difference of wave pattern between the two VLCC models is within the uncertainty level of the present measurement. The Froude number of the VLCCs was 0.142, resulting in the short waves with the relatively small wave heights. It is observed that the bow wave is dominant and small short waves follow. For the VLCCs, the contour levels of measured wave height in Fig. 9 are a quarter of those in Fig. 7 of the KCS case.

The wave resistance of this low-speed ship is usually negligible; however, the big bow wave associated with wave-breaking phenomena of real ships sometimes draw attention. However, for the present VLCC hull forms in the model scale, wave breaking was not observed. Transverse wave components are hardly identified. Short divergent wave components exist along the edge of the Kelvin triangle. The present VLCCs have the design waterline located above the transom, although there is apparently no transom effect. But the local flow measurement revealed that the flow angle seemed to undergo an abrupt change due to the transom with flow reversal.

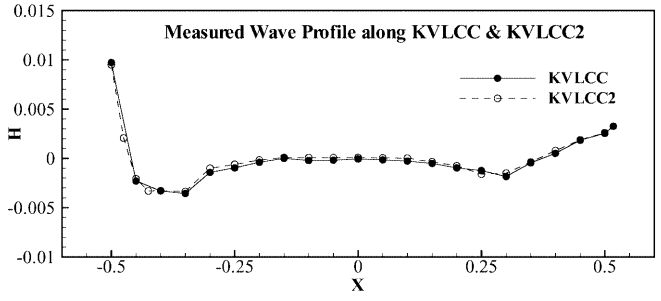

Fig. 8. Measured wave elevation along KVLCC and KVLCC2 ($Fn = 0.142$)

4.2
Local mean velocity fields

Most of drag occurs due to viscosity for modern commercial ships with moderate or low speed. Viscous drag is dependent on velocity profile and pressure distribution inside the turbulent boundary layer. To understand the relation between hull form and viscous drag, boundary layer flows should be explored. Furthermore, the velocity distribution in the stern region is very important to design the proper propeller with high efficiency, since the propulsor of a modern commercial ship operates inside the wake behind stern bulb.

A thin boundary layer is formed in the forebody of the ship. Flow angles are dependent on the shape of the bulbous bow and shoulder in the forebody. The boundary layer becomes thicker along the hull surface and parallel in the midship region. Flows are swept upwards from the bottom in the stern bilge region, where bilge vortices are formed. For fine slender ships like the KCS, the weak bilge vortices are found at the propeller plane. However, if the sectional area change is large at the stern, as in the case of VLCCs, strong bilge vortices can be located inside the propeller plane. The location and strength of these bilge vortices play the key role in determining the nominal wake distribution and the resulting propulsive efficiency.

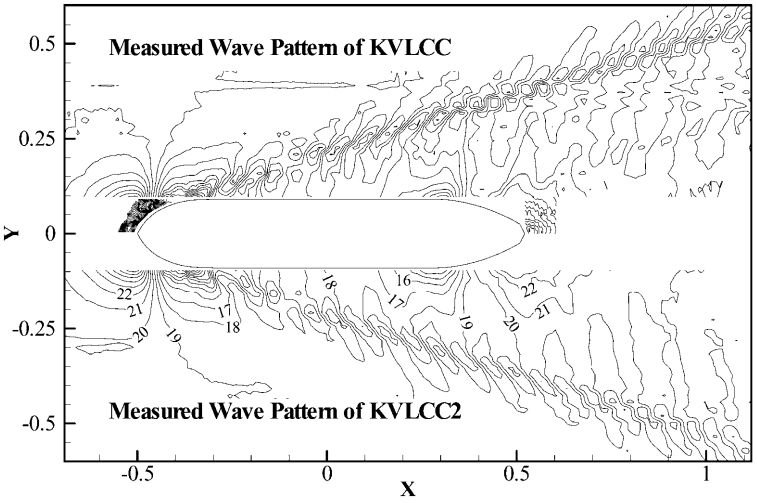

Level	H
73	0.014
69	0.013
65	0.012
61	0.011
57	0.010
53	0.009
49	0.008
45	0.007
41	0.006
37	0.005
33	0.004
29	0.003
25	0.001
21	0.000
17	-0.001
13	-0.002
9	-0.003
5	-0.004
1	-0.005

Fig. 9. Measured wave pattern around KVLCC and KVLCC2 ($Fn = 0.142$)

As mentioned earlier, the two VLCC hull forms have the same forebody and slightly different afterbodies. The difference in wake distribution of KVLCC and KVLCC2 will provide valuable information to explore the influence of stern frame line change on wake distribution. Viscous flow solvers can be applied in the initial hull form design to predict the turbulent boundary layer and the wake around a ship. However, before practical application of such computational tools, they should be validated with the reliable data of realistic hull forms. The present experimental data will provide good test cases to ascertain whether physical and numerical modeling can predict boundary layer and wake flows around modern hull forms.

4.2.1
The KCS case

The mean velocity components around the stern region of the KCS model are shown in Fig. 10. Five stern stations (St. 2, 1, 0.35, −0.5767, −2) of $X = 0.4$, 0.45, 0.4825, 0.5288, and 0.6 were chosen for the stern flow measurement around a modern container ship. A dummy hub was attached to prevent the abrupt change after stern boss. The measurement was carried out across the center plane to confirm the symmetry of flow. Axial velocity contours and transverse vectors show good symmetry with respect to the $Y = 0$ plane. The notable fact in the axial velocity contours at $X = 0.4$ is a thick boundary layer on the concave surface. It is likely that streamlines from bilge area converge onto the concave surface after the midship, resulting in a thickening of the boundary layer thereafter. It is also observed that the boundary layer is very thin along the convex keel region, since low-momentum fluids are moved towards the concave side.

The axial velocity contours at the propeller plane ($X = 0.4825$) are of round shape, which is favorable to the propeller efficiency. The stern bulb clearly affected the wake distribution at the propeller plane. A very weak vortex near the upper corner of the propeller hub is observed, however, the strength is too small to identify from the figure. It is likely that the transverse flow at the propeller plane is not rolled up enough to form a discrete vortex in the KCS case due to the fine stern shape. The

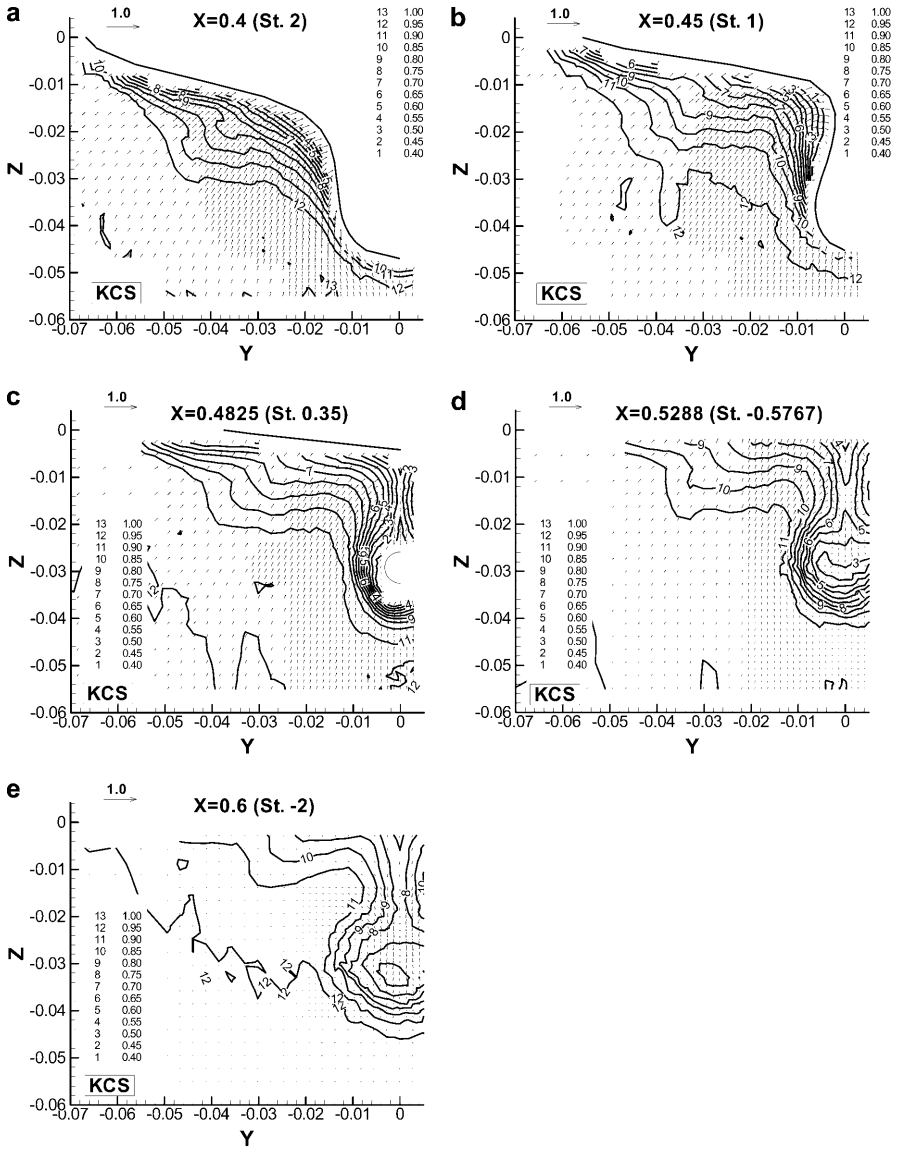

Fig. 10a–e. Measured mean velocity fields around KCS. **a** $X = 0.4$ (St. 2), **b** $X = 0.45$ (St. 1), **c** $X = 0.4825$ (St. 0.35), **d** $X = 0.5288$ (St. −0.5767), **e** $X = 0.6$ (St. −2)

shaft centerline of the model container ship was located at $Z = -0.02913$, where the propeller with the radius $R_P = 0.03435$ (i.e., 7.9 m for the prototype and 25 cm for the model ship) would be located. The propeller hub is marked as a semi-circle in Fig. 10c. The transverse velocity vectors at $X = 0.5288$ in the wake region illustrate the vortex more clearly than in the propeller plane. The next station at $X = 0.6$ shows the wake field diffusing slowly.

Velocity profiles at the propeller plane are measured separately using a nominal wake-measuring device using the same Pitot tubes. Details of nominal wake distribution are given in Fig. 11. The measured propeller plane wake is shown in local propeller coordinates (Y_P, Z_P), where the inner and outer circles denote 30% and 110% of the propeller radius (R_P), respectively. The axial velocity contours show the near-wake field behind the stern bulb. Most transverse flow vectors are directed upward and inward, as expected from hull tangents in the stern region. Downward flow vectors are observed above the hub along the plane of symmetry and the transverse velocity vectors shows weak bilge vortices.

4.2.2
The KVLCC and KVLCC2 cases

For the VLCCs, the stern boss cap of the semi-sphere was attached instead of a dummy hub, since the hub made it difficult to measure the velocity around the shaft centerline. The propeller plane ($X = 0.4825$, St. 0.35) was located just behind the stern cap. The shaft centerline of the VLCCs was located at $Z = -0.04688$. The measured mean velocity components around the stern region of KVLCC and KVLCC2 are compared in Fig. 12. Mean velocity fields were measured at six stern stations (St. 3, 2, 1, 0.35, −0.4525, −2) of $X = 0.35$, 0.4, 0.45, 0.4825, 0.5226, and 0.6

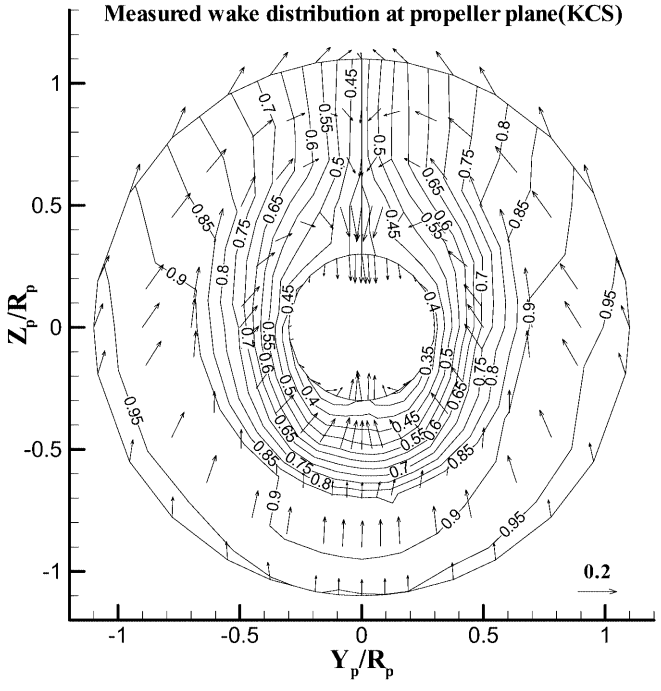

Fig. 11. Measured wake distribution of KCS at the propeller plane

for both KVLCC and KVLCC2. It is seen that a thicker boundary layer than in the previous KCS case is formed on the concave surface with low-momentum fluids fed from the bilge region. It is likely that the trace of the full midship section still remains for both ships. There is not a big difference before $X = 0.45$ between the two VLCC hull forms.

A distortion of axial velocity contours is found just above the stern bulb at $X = 0.45$. The boundary layer profiles of KVLCC2 show more distortion than those of KVLCC, as expected from the stronger turn of the bilge shape. At $X = 0.4825$, the distortion of axial velocity contours is clearly observed near the stern bulb ($Z = -0.04$, $Y = -0.015$) of both ship models. The strong distortion of axial velocity contours implies the formation of bilge vortices. Both ships show hook-like axial velocity contours and strong transverse vortical flows are seen. The distortion of velocity contours is severer in KVLCC2, implying that stronger bilge vortices are formed. The formation of longitudinal vortices are well identified in the axial vorticity contours at $X = 0.4825$ given in Fig. 13. A vortex core is more clearly seen in KVLCC2, while KVLCC has a narrower vortex region. Two contra-rotating bilge vortices are formed since the hull form is symmetric with respect to $Y = 0$ plane. The relationship between the stern hull form and the strength and location of bilge vortices is very important in hull form design, since it will determine the inflow to the propeller blades.

There are kinks in the axial velocity contours at $Y = -0.04$ of the $X = 0.4825$ plane of KVLCC. However, it is believed that these arise from possible errors in data acquisition or the location of probes during the experiment, and thus should be ignored. It should be noted that the measurement points with local flow angle larger than ±40° are discarded since they are outside the calibration range. This occurred below the stern cap and behind the transom.

It is noteworthy that low-momentum fluids accumulate near the free surface. A thick boundary layer is already observed at $X = 0.45$ and $X = 0.4825$ near the free surface. A weak vortical structure in the axial vorticity contours in Fig. 13 is found. This thick boundary layer near the water plane was also reported in the wind tunnel measurement for KVLCC2 (Van et al. 1999); thus, it is certain that these low-momentum fluids do not stem from the free-surface effect. Moreover, the Froude number of the present cases is very low ($Fn = 0.142$). It is believed that the thick boundary layer near the water plane is due to flow convergence along the upper edge of hollow stern frame lines.

The near wake regions of $X = 0.5226$ and $X = 0.6$ planes show wake pattern. The axial velocity component in the centerline is recovered up to 0.7 at $X = 0.6$. As the flow goes downstream, the shear layer of wake flow is expanded and the center of longitudinal vortex moves downward. This can be explained with the entrainment of inviscid flow into the wake region. The velocity outside the longitudinal vortex region increases, while the retarded flow in the core of wake is moved downward. Thick boundary layers near the water plane still exist and diffuse slowly.

The axial velocity at the propeller plane is extracted and compared in Fig. 14. KVLCC has more vertical contour

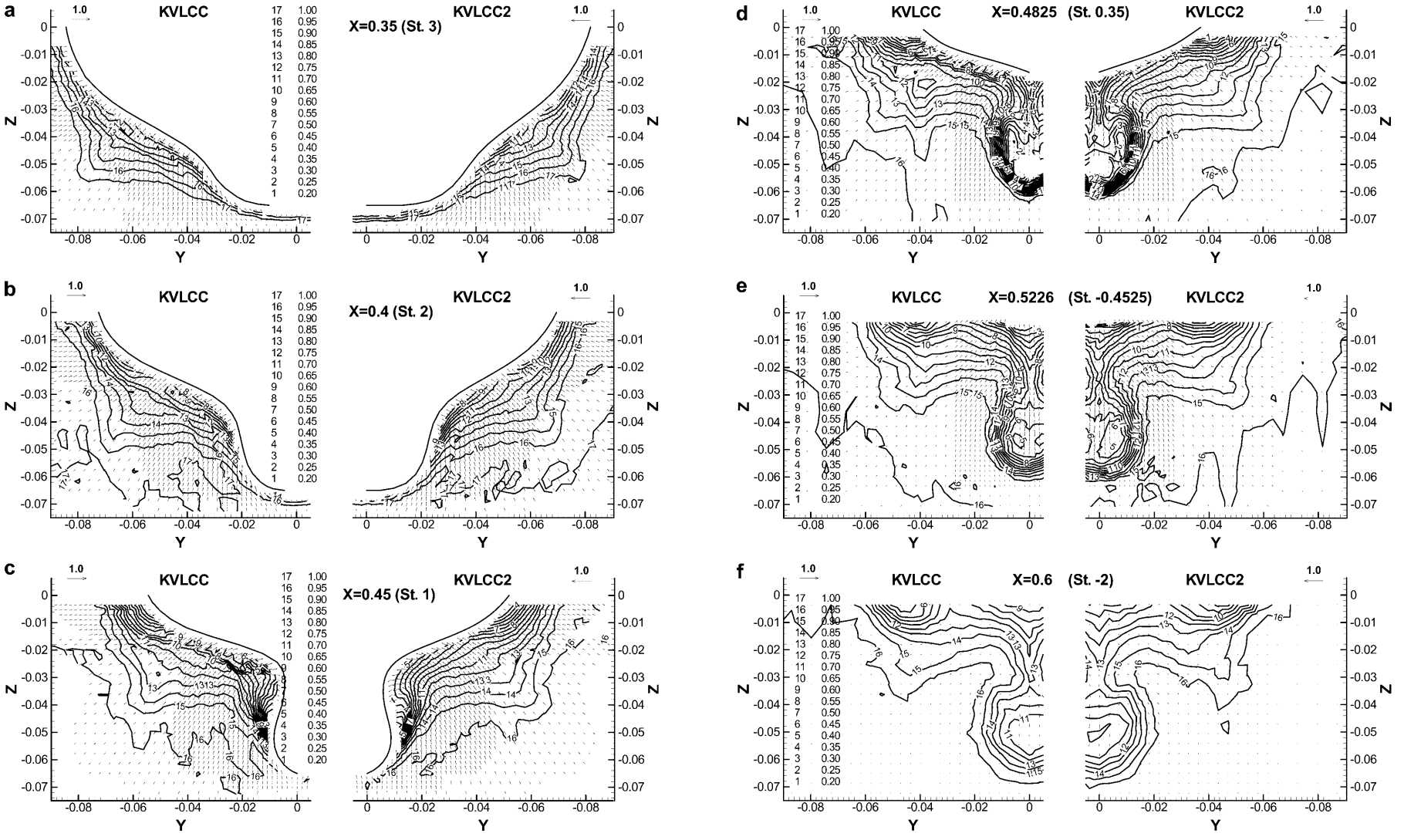

Fig. 12a–f. Measured mean velocity fields around KVLCC and KVLCC2. **a** $X = 0.35$ (St. 3), **b** $X = 0.4$ (St. 2), **c** $X = 0.45$ (St. 1), **d** $X = 0.4825$ (St. 0.35), **e** $X = 0.5226$ (St. −0.4525), **f** $X = 0.6$ (St. -2)

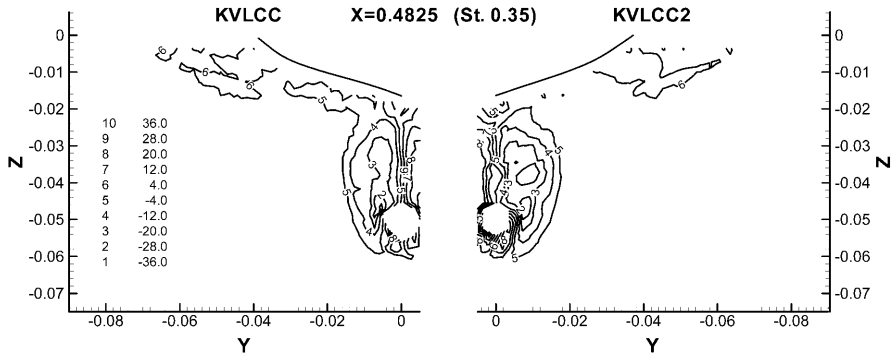

Fig. 13. Axial vorticity contours around KVLCC and KVLCC2 at X = 0.4825

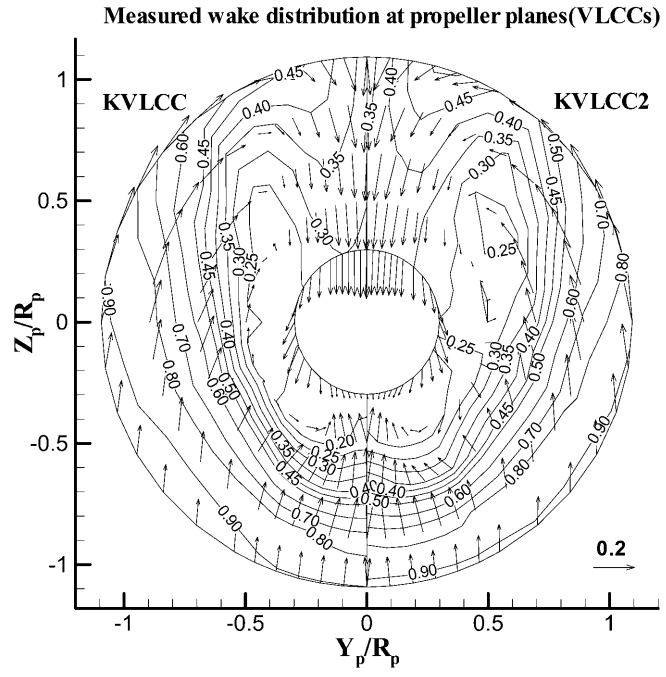

Fig. 14. Propeller plane wake distribution of KVLCC and KVLCC2

shapes than KVLCC2. The depth of hook is clearer at $U = 0.4$ and 0.35 contours of KVLCC2. This difference in nominal wake distribution will contribute a notable change of the propulsive efficiency. It should be mentioned that velocities at some locations below stern cap in the propeller plane could not be determined since the local flow angle was out of calibration range. Thus, the velocity components at the lower part of 0.3 R_p and 0.4 R_p position is extrapolated. However, authors believe that the extrapolation does not affect the results much. The shape of axial velocity contours of KVLCC2 in Fig. 14 shows clearer hook shape and becomes closer to a concentric circle than KVLCC. Moreover, the nominal wake fraction at the propeller plane of KVLCC2 is larger due to the U-shaped stern frame lines. This distribution is more favorable and preferable for higher propulsive efficiency, although strong bilge vortices can increase the form drag of a ship.

Resistance and self-propulsion test results confirmed the above observations. The same ship models used for local measurement were used for the self-propulsion test with a stock propeller, which was previously used for other VLCCs with similar wake distribution. The diameter of the propeller is 0.0308125 (i.e., 9.86 m for the real ship and 0.17 m for the model ship). Full-scale prediction was performed following the ITTC method (ITTC 1999). The results are compared at the design speed (15.5 knots) in Table 4. The resistance of KVLCC2 is slightly greater than that of KVLCC due to the generation of stronger bilge vortices. However, the quasi-propulsive efficiency of KVLCC2 is higher due to the favorable wake distribution. The effective wake of KVLCC2 is larger than that of KVLCC and the hull efficiency is higher for KVLCC2. Consequently, slightly less power is required for KVLCC2.

As noted earlier, the difference in stern hull forms of KVLCC and KVLCC2 is as much as shipyards usually apply for hull form optimization. The global features of the stern flows are similar, however, the changes of flow are notable at the propeller plane. It will be very interesting to see whether the numerical modeling can tell the difference in the propeller plane wake of KVLCC and KVLCC2.

5
Concluding remarks

In order to provide a benchmark database for CFD validation in ship hydrodynamics, global force, wave pattern, and local mean velocity components around a 3,600-TEU container ship model (KCS) and two 300K VLCC models (KVLCC and KVLCC2) were measured in the towing tank. These hull forms are very similar to commercial ships of today. Focus was directed on wave generation on the free surface for the KCS, while for the KVLCC and KVLCC2, the formation of bilge vortices and the wake difference between two similar tanker hull forms were emphasized.

Table 4. Resistance and propulsive coefficients of KVLCC and KVLCC2 (Vs = 15.5 knots)

Ship	Cr (X1000)	EHP (PS)	DHP	w_M	w_S	t	η_H	η_R	η_O	η_D
KVLCC	0.638	18,223	25,467	0.407	0.297	0.197	1.142	1.005	0.624	0.716
KVLCC2	0.660	18,438	25,384	0.443	0.305	0.190	1.165	1.005	0.620	0.726

For KCS with moderate Froude number ($Fn = 0.26$), wave patterns composed of transverse and divergent wave components were clearly seen. However, a complicated unstable transom wave field was observed, although the transom stern was located initially above the design waterline. For KVLCC and KVLCC2 with low Froude number ($Fn = 0.142$) and full bow hull form, a big bow wave was observed followed by small short waves.

Measured velocity components revealed the boundary layer structure developing over the stern and evolving into a complicated three-dimensional wake flow. A thick boundary layer was formed along the concave surface in the stern region. A weak vortex was observed with a thick boundary layer near the free surface. For the KCS with a fine stern shape, the formation of bilge vortices was not so prominent. However, in the case of the VLCCs, strong bilge vortices were formed and distorted the axial velocity profiles in the propeller plane. The difference in wake distribution and its relation to propulsive efficiency was also explored from the viewpoint of stern hull form modification.

The experimental data presented in the paper were recommended as a benchmark database by the International Towing Tank Conference and used as test cases in the Gothenburg 2000 CFD Workshop in Ship Hydrodynamics. The authors believe that the present experimental data can be used in evaluating physical and numerical modeling to predict wave generation on the free surface and three-dimensional boundary layer and wake around modern commercial ships with bow and stern bulb.

References

Bertram V; Chao K-Y; Lammers G; Laudan J (1994) Experimental validation data of free-surface flows for cargo vessels. In: Kodama Y (ed) Proceedings of CFD Workshop, 1994, Tokyo, Japan. pp 311–320

Coleman HW; Steele WG (1999) Experimentation and uncertainty analysis for engineers. Wiley-Interscience, New York

Denker J; Knaack T; Kux J (1992) Experimental and numerical investigations of HSVA-tanker 2 flow field. Report 521, Uni. Institute of Shipbuilding (IfS), Hamburg, Germany

Dyne G (1995) An experimental investigation of the tanker model 'Dyne' in a towing tank. Report CHA/NAVR/-95/0036. Chalmers University of Technology, Sweden

Fry DJ; Kim YH (1985) Bow flow field fo surface ships. In: Proceedings of the 15th ONR Symposium on Naval Hydrodynamics, 1985, Hamburg, Germany

Fujisawa J; Ukon Y; Kume K; Takeshi H (2000) Local velocity field measurements around the KCS Model (SRI M.S.No.631) in the SRI 400 m towing tank. Ship Performance Division Report No. 00–003–02. The Ship Research Institute of Japan, Mitaka, Japan

Gietz U; Kux J (1995) Flow investigations on the Hamburg test case model in the wind tunnel. (in German) Report 550, Uni. Hamburg. Institute of Shipbuilding (Ifs), University of Hamburg, Hamburg, Germany

ITTC (1999) Quality manual. In: Yang SI (ed) Proceedings of the 22nd International Towing Tank Conference (ITTC), 1999, Seoul, Korea/Shanghai, PR China

Kang K; et al. (1998) The influence of the stern frame shape for a high-speed container ship on the powering performance. In: Oosterveld MCW, Tan SG (eds) Proceedings of the 7th International Symposium on Practical Design of Ships and Mobile Units (PRADS), 1998, The Hague, The Netherlands. pp 691–698

Kim WJ; et al. (1997) Study on calibration method of five-hole Pitot probes for wake measurements. (in Korean) J Soc Nav Archit Korea 34: 11–19

Knaack T (1992) Investigation of structure of Reynolds tensor fields in a three-dimensional flow. (in German) Report 527, University of Hamburg. Institute of Shipbuilding (IfS), University of Hamburg, Hamburg, Germany

Kodama Y (ed) (1994) Proceedings of CFD workshop, Tokyo, Japan

Larsson L; Patel VC; Dyne G (1991) Ship viscous flow. In: Larsson L, Patel VC, Dyne G (ed) Proceedings of SSPA-CTH-IIHR Workshop, 1990, Gothenburg, Sweden

Larsson L; Stern F; Bertram V (2000) Gothenburg 2000: a workshop on numerical ship hydrodynamics. Gothenburg, Sweden; (see also http://www.iihr.uiowa.edu/gothenburg2000/V)

Lee J; Lee SJ; Van SH (1998) Wind tunnel test on a double-deck-shaped ship model. In: Kim H, Lee SH, Lee SJ (eds) Proceedings of the 3rd International Conference on Hydrodynamics (ICHD), 1998, Seoul, Korea. pp 815–820

Longo J; Stern F (1996) Technical note: evaluation of surface-ship resistance and propulsion model-scale database for CFD validation. J Ship Res 40: 112–116

Longo J; Stern F (1999) Resistance, sinkage and trim, wave profile, and nominal wake and uncertainty assessment for DTMB model 5512. In: Proceedings of the 25th ATTC, 1999, Iowa City, USA

Longo J; Stern F; Toda Y (1993) Mean-flow measurements in the boundary layer and wake and wave field of a Series 60 C_B=0.60 ship model – Part 2: scale effects on near-field wave patterns and comparisons with inviscid theory. J Ship Res 37: 16–24

Ogiwara S (1994) Stern flow measurements for the tanker 'Ryuko-Maru' in model-scale, intermediate-scale, and full-scale ships. In: Kodama Y (eds) Proceedings of CFD Workshop, vol. 1, 1994, Tokyo, Japan. pp 341–349

Olivieri A; Penna R (1999) Uncertainty assessment in wave elevation measurements. In: ISOPE, 1999, Brest, France

Ratcliffe T (1998) http://www50.dt.navy.mil/5415/
Society of Naval Architect and Marine Engineers (SNAME) (1967) Principles of naval architecture. Society of Naval Architect and Marine Engineers (SNAME), Jersey City, NJ

Stern F; Longo J; Maksoud M; Suzuki T (1998) Evaluation of surface-ship resistance and propulsion model-scale database for CFD validation. In: Proceedings of the 1st Symposium on Marine Applications of Computational Fluid Dynamics, 1998, McLean, USA

Suzuki H; Suzuki T; Miyazaki S (1997) Turbulence measurements in stern flow field of a ship model – series 60, C_B=0.60. (in Japanese) J Kansai Soc Nav Archit 227: 29–40

Suzuki H; Miyazaki S; Suzuki T; Matsumura K (1998) Turbulence measurements in stern flow field of two ship models. In: Himeno Y (ed) Proceedings of the 3rd Osaka Colloquium on Advanced CFD Applications to Ship Flow and Hull Form Design, 1998, Osaka, Japan. pp 229–240

Toda Y; Stern F; Tanaka I; Patel VC (1990) Mean-flow measurements in the boundary layer and wake of a series 60 C_B=0.60 model ship with and without propeller. J Ship Res 34(4): 225–252

Toda Y; Stern F; Longo J (1992) Mean-flow measurements in the boundary layer and wake and wave field of a series 60 C_B=0.60 ship model – Part 1: Froude numbers 0.16 and 0.316. J Ship Res 36: 360–377

Tsukada Y; Hori T; Ukon Y; Kume K; Takeshi H (2000) Surface pressure measurements on the KCS model (SRI M.S.No.631) in the SRI 400 m towing tank. Ship Performance Division Report No. 00–004–01. The Ship Research Institute of Japan, Mitaka, Japan

Van SH; Park YJ (1993) Uncertainty analysis for the experiments in KRISO towing tank. (in Korean) J Ships Ocean Eng 16: 60–70

Van SH; Kim WJ; Kim HR; Lee SJ (1999) Wind tunnel test on flow characteristics of KRISO 300 K VLCC double model. In: Naito S, Choi HS (eds) Proceedings of the 4th Japan-Korea Joint Workshop on Marine & Ship Hydrodynamics (JAKOM), 1999, Fukuoka, Japan. pp 157–164